ADVANCED MATERIALS
www.advmat.de

Ultrastrong Bioinspired Graphene-Based Fibers via Synergistic Toughening

*Yuanyuan Zhang, Yuchen Li, Peng Ming, Qi Zhang, Tianxi Liu, Lei Jiang, and Qunfeng Cheng**

Graphene-based fibers (GBFs) are an ideal bridge for integrating the extraordinary properties of individual graphene nanosheets into advanced, macroscopic, and functional materials for practical applications, especially in flexible energy-storage and intelligent devices.[1] GBFs were first demonstrated through wet-spinning graphene oxide (GO) nanosheets in 2011 by Xu and Gao.[2] However, this kind of GBFs show poor mechanical properties with only tensile strength of 140 MPa, and electrical conductivity of 250 S cm^{-1}. Numerous strategies have been attempted to improve the mechanical properties of GBFs through new fabrication techniques, mainly from the following three aspects:

i) Assembly control. For example, Dong et al.[3] assembled GBFs by using an one-step dimensionally confined hydrothermal strategy and achieved a tensile strength of 420 MPa. Cao et al.[4] developed a "programmable writing" technique for the fabrication of GBFs with 365 MPa. Cruz-Silva et al.[5] scrolled GO film into GBFs with only 39.2 MPa, and further annealed GBFs at 2800 °C to achieve high electrical conductivity of 416 S cm^{-1}.
ii) Interface engineering. Divalent ions, such as Ca^{2+}[6] and Mg^{2+},[7] were introduced to form ionic bonding with GO nanosheets in GBFs, resulting in high tensile strength and high toughness of 501.5 MPa and of 16.8 MJ m^{-3}, respectively.
iii) Polymer reinforcement. For example, Jalili et al.[8] applied chitosan to obtain high tensile strength of 442 MPa. Hu et al.[9] grafted hyperbranched polyglycerol (HPG) onto GO nanosheets, and further developed a technique that uses glutaraldehyde (GA) to form covalent acetal bridges between –OH groups of HPG and GO nanosheets, resulting in a high tensile strength of 652 MPa. Other polymers, including polyacrylonitrile,[10] poly(vinyl alcohol) (PVA),[11] and poly(glycidyl methacrylate) (PGMA),[12] have also been used to reinforce GBFs.

Although the mechanical properties of resultant GBFs have been improved, the highest tensile strength of GBFs ever reached to date is 652 MPa,[9] possibly attributable to weak interface interactions in GBFs, leading to inefficient loading transfer. Thus, it still remains a challenge to design and fabricate GBFs with high mechanical properties. On the other hand, natural nacre, whose extraordinary mechanical properties are due to its hierarchical micro/nanoscale structure and abundant interface interactions,[13] offers an ideal model for constructing high-performance graphene-based composites,[14] especially for GBFs.

In our work, inspired by the interface interactions of natural nacre, we demonstrate ultrastrong GBFs by constructing synergistic interface interactions of ionic bonding with Ca^{2+}, and covalent bonding with 10,12-pentacosadiyn-1-ol (PCDO). The tensile strength and toughness of bioinspired GBFs reach as high as 842.6 MPa and 15.8 MJ m^{-3}, respectively, and are superior to all other reported GBFs. In addition, the electrical conductivity of bioinspired GBFs, which can be as high as 292.4 S cm^{-1}, also exceeds the performance of neat GBFs.[2] Such high performance readily lends bioinspired GBFs to integration in a diverse variety of applications, such as flexible electrodes in wearable and intelligent devices, including actuators, motors, and robots. This bioinspired synergistic toughening strategy also provides a new insight for constructing integrated high-performance GBFs in the near future.

The GO nanosheets, prepared according to modified Hummer's method, show the thickness of 0.75 nm (Figure S1, Supporting Information) and the average size of 30.5 μm with a distribution ranging from several micrometers (down to 10.5 μm) to hundred micrometers (up to 103.5 μm) (Figure S2, Supporting Information). The process for the preparation of bioinspired GBFs is illustrated in **Figure 1**a. First, the GO fiber was assembled by the wet-spinning process. The as-prepared spinning dope with a GO concentration of ≈10 mg mL^{-1} was continuously injected into a rotating coagulation bath with an ethanol–water (1:3 in volume) solution containing 5 wt% $CaCl_2$. After immersing in the coagulation bath for ≈30 min the GO-Ca^{2+} fiber was transferred into an ethanol–water solution to remove the residual salts. After drying at room temperature for several hours, the GO-Ca^{2+} fiber was transferred into an oven for further annealing at 40, 80, 120, and 160 °C, resulting in GO-Ca^{2+}-I, GO-Ca^{2+}-II, GO-Ca^{2+}-III, and GO-Ca^{2+}-IV, respectively. These

Dr. Y. Y. Zhang , P. Ming, Q. Zhang, Prof. L. Jiang, Prof. Q. F. Cheng
Key Laboratory of Bio-inspired Smart Interfacial Science and Technology of Ministry of Education
School of Chemistry and Environment
Beihang University
Beijing 100191, P. R. China
E-mail: cheng@buaa.edu.cn
Y. C. Li
Beijing Engineering Research Center of Printed Electronics
Beijing Institute of Graphic Communication
Beijing 102600, P. R. China
Prof. T. X. Liu
State Key Laboratory for Modification of Chemical Fibers and Polymer Materials
Donghua University
Shanghai 201620, P. R. China

DOI: 10.1002/adma.201506074

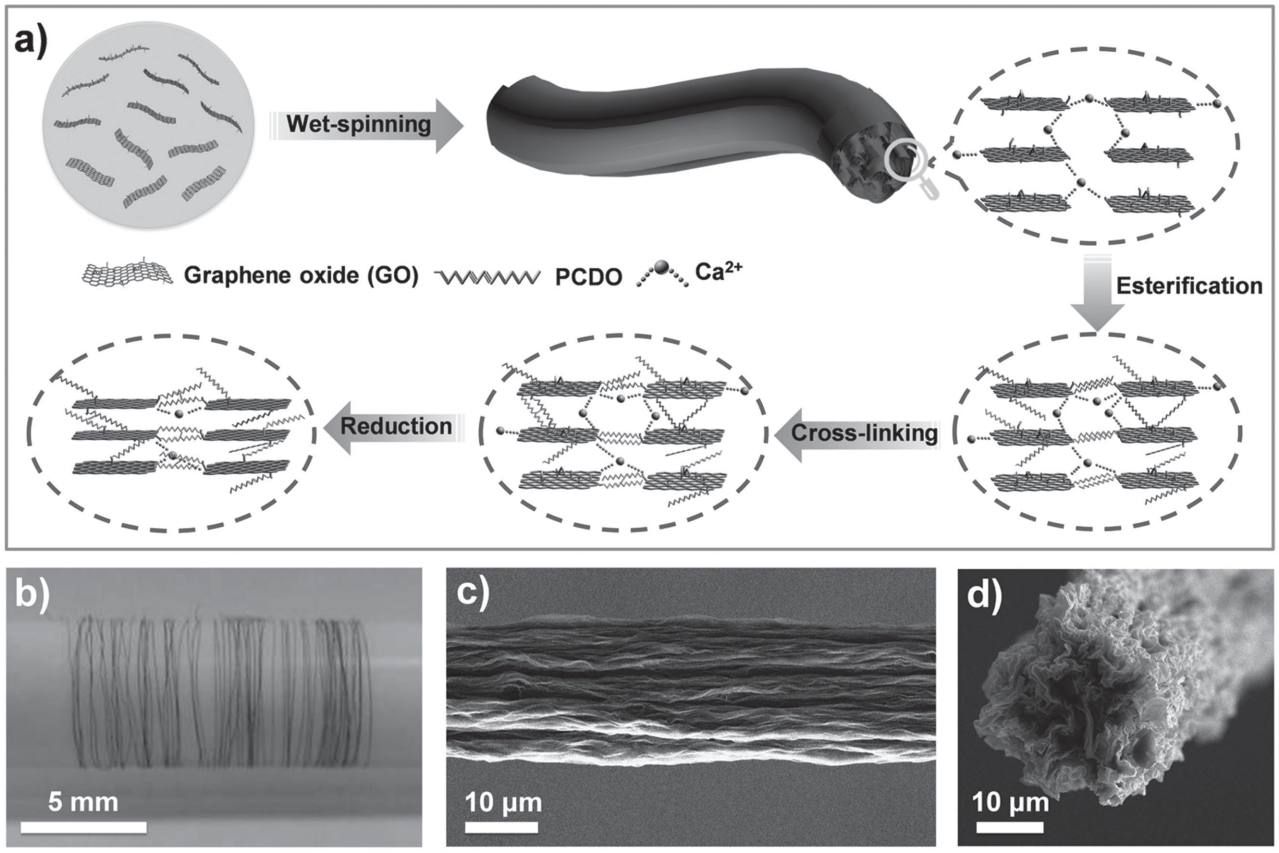

Figure 1. Schematic illustration of the preparation process for the bioinspired rGO-Ca^{2+}-PCDO fibers. a) The GO-Ca^{2+} fibers were assembled through the wet-spinning method in one step, followed by PCDO grafting. Under UV irradiation, the PCDO molecules were cross-linked together between adjacent GO nanosheets. Finally, the GO-Ca^{2+}-PCDO fiber was chemically reduced by HI. The ultrastrong bioinspired rGO-Ca^{2+}-PCDO fiber was obtained. b) Digital photographs of bioinspired rGO-Ca^{2+}-PCDO fiber. c,d) SEM images of surface morphology and cross-section of a bioinspired rGO-Ca^{2+}-PCDO fiber.

GO-Ca^{2+} fibers were grafted with PCDO through dip-coating with a PCDO/tetrahydrofuran solution. Under UV irradiation, the PCDO molecules were cross-linked by a 1,4-addition polymerization of their diacetylenic units.[15] Finally, these GO-Ca^{2+}-PCDO fibers were chemically reduced by hydroiodic (HI) acid, and then washed by ethanol and water to remove the residual iodine. The corresponding bioinspired GBFs (chemically reduced GO (rGO)-Ca^{2+}-PCDO-I, rGO-Ca^{2+}-PCDO-II, rGO-Ca^{2+}-PCDO-III, and rGO-Ca^{2+}-PCDO-IV) were then obtained, as shown in Figure 1b. The surface morphology and cross-section morphology of bioinspired rGO-Ca^{2+}-PCDO fibers are shown in Figure 1c,d, respectively.

In this study, the amount of PCDO grafted onto the GO nanosheets can be tuned by annealing GO nanosheets at different temperatures to remove specific oxygen-containing functional groups from the surface of GO nanosheets, which can be verified by the X-ray photoelectron spectroscopy (XPS), as shown in Figure S3 in the Supporting Information. The ratio of C to O increases from 3.0 for GO-Ca^{2+}-I to 6.35 for GO-Ca^{2+}-IV, as listed in Table S1 in the Supporting Information. The dehydration of the GO-Ca^{2+} fiber, driven by the annealing process, results in a decrease of the *d*-spacing, which can be confirmed through X-ray diffraction (XRD) spectra, as shown in Figure S4 in the Supporting Information. For example, the *d*-spacing of GO-Ca^{2+}-I fiber decreased from 8.95 to 7.78 Å for GO-Ca^{2+}-III, as listed in Table S2 in the Supporting Information. When the annealing temperature is further increased, the oxygen-containing groups are partly destroyed,[16] limiting the amount of esterification with PCDO molecules. Thus, the content of PCDO molecules in GO-Ca^{2+}-PCDO fibers decreases, confirmed by thermogravimetric analysis (TGA), as shown in Figure S5 in the Supporting Information. The specific amounts of PCDO molecules in resultant GBFs are listed in Table S3 in the Supporting Information. Fourier transform infrared spectroscopy (FTIR) was conducted to verify the chemical reaction between GO nanosheets with PCDO molecules in the GO-Ca^{2+}-PCDO fibers, as shown in **Figure 2**a. The FTIR spectra of all GO-Ca^{2+} fibers and GO-Ca^{2+}-PCDO fibers are shown in Figure S6 in the Supporting Information. The C=O stretching vibration bands in carboxyl groups of GO are observed at 1730 cm^{-1} in GO-Ca^{2+} fiber. After esterification with PCDO, the peak at 1730 cm^{-1} is weakened, and is accompanied by a peak at 1770 cm^{-1} that corresponds to the stretching vibration of the C=O moiety in ester groups, especially for rGO-Ca^{2+}-PCDO fiber. This indicates that PCDO molecules have been stably grafted onto the GO sheets, even after HI reduction.[15] The covalent bonding

Adv. Mater. **2016**,
DOI: 10.1002/adma.201506074

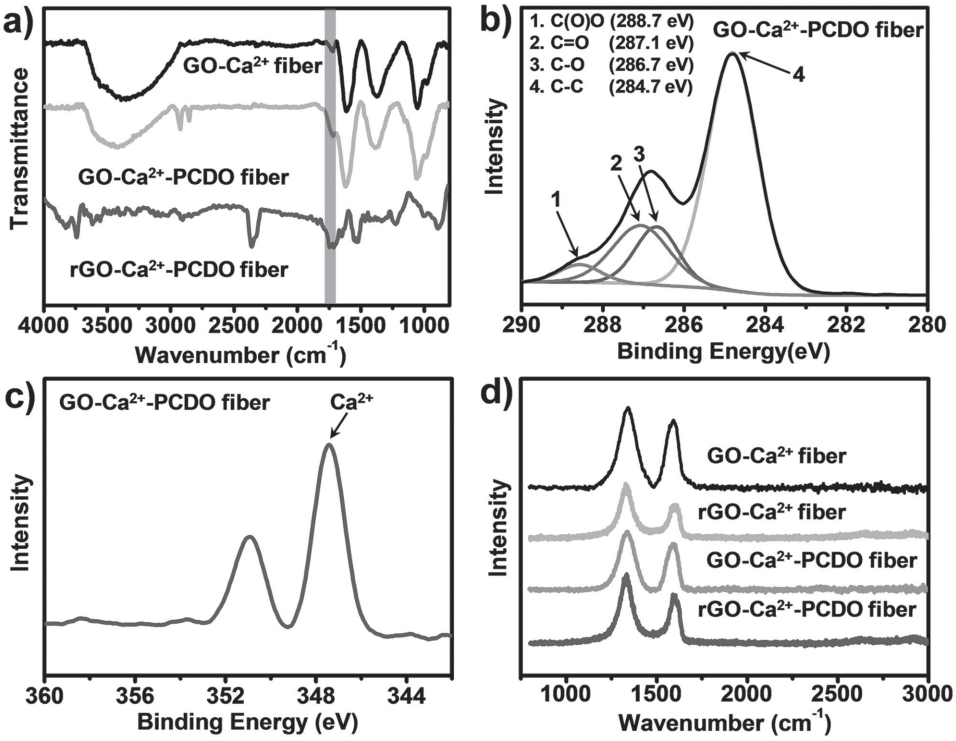

Figure 2. a) FTIR spectra of GO-Ca^{2+}, GO-Ca^{2+}-PCDO, and rGO-Ca^{2+}-PCDO fibers. The peak at 1770 cm^{-1} corresponding to the stretching vibration of the C=O moiety in ester groups indicates PCDO has been successfully grafted onto the GO nanosheets. b) The XPS spectrum of GO-Ca^{2+}-PCDO fiber indicates an apparent decrease of C_{1s} peak in the epoxy/ether group, and an increase of C_{1s} in the hydroxyl/alkoxide group, verifying the ring-opening reaction of epoxides on the GO nanosheets. c) The decrease in binding energy of the $Ca_{2p3/2}$ in $CaCl_2$ supplies direct evidence to the formation of divalent ionic bonding between GO nanosheets and Ca^{2+} ions. d) Raman spectra of GO-Ca^{2+}, rGO-Ca^{2+}, GO-Ca^{2+}-PCDO, and rGO-Ca^{2+}-PCDO fibers show the increase of I_D/I_G ratio after HI reduction, verifying the restoration and homogenization of sp^2-hybridized carbons after HI reduction.

between PCDO and GO nanosheets can also be confirmed with XPS, as shown in Figure 2b. C_{1s} peak shows an apparent decrease in the epoxy/ether group, and an increase in the hydroxyl/alkoxide group, demonstrating the ring-open reaction of epoxides of GO nanosheets.[14] Meanwhile, the Ca^{2+} signals of GO-Ca^{2+}-PCDO fiber are also detected, as shown in Figure 2c, further indicating the modification of the ionic bonding between adjacent GO nanosheets. In addition, the elemental mapping of GO-Ca^{2+}-PCDO fiber indicates that Ca element is homogeneously distributed in the fiber (Figure S7, Supporting Information). After HI reduction, the Ca element content in the fiber decreases due to the removal of original oxygen containing groups on GO nanosheets, but Ca element is still homogeneously distributed in the fiber, as shown in Figure S8 in the Supporting Information, which further confirms the formation of ionic bonding between adjacent GO nanosheets with Ca^{2+}. The Raman spectra shown in Figure 2d demonstrate that the relative peak intensity ratio of D band to G band (I_D/I_G) is increased from 1.61 for GO-Ca^{2+}-II fiber to 1.63 for GO-Ca^{2+}-PCDO-II fiber, as listed in Table S4 in the Supporting Information. And the I_D/I_G ratio increases from 1.83 for rGO-Ca^{2+}-II fiber to 1.90 for rGO-Ca^{2+}-PCDO-II fiber, verifying the restoration and homogenization of sp^2 hybridized carbons after HI reduction.[17]

The typical tensile stress–strain curves of GO-Ca^{2+}-II fiber (curve 1), rGO-Ca^{2+}-II fiber (curve 2), GO-Ca^{2+}-PCDO-II fiber (curve 3), and rGO-Ca^{2+}-PCDO-II fiber (curve 4) are shown in **Figure 3**a. All the stress–strain curves corresponding to GO-Ca^{2+} fiber, rGO-Ca^{2+} fiber, GO-Ca^{2+}-PCDO fiber, and rGO-Ca^{2+}-PCDO fiber are shown in Figure S9–S11 in the Supporting Information, respectively. The GO-Ca^{2+}-II fiber possesses tensile strength of 390.1 ± 18.5 MPa and toughness of 2.4 ± 0.4 MJ m^{-3}, consistent with previous reports.[8] After HI reduction, the tensile strength and toughness of rGO-Ca^{2+}-II fiber are improved to 500.5 ± 10.9 MPa and 12.0 ± 1.5 MJ m^{-3}, respectively, comparable to the GO fiber assembled from giant GO nanosheets.[6] This improvement is attributed to the introduction of ionic bonding by the Ca^{2+} metal cation in the coagulation process.[18] The tensile strength and toughness of GO-Ca^{2+}-PCDO-II fiber reach 610.8 ± 17.5 MPa and 2.7 ± 0.2 MJ m^{-3}, respectively. After HI reduction, the tensile strength and toughness of rGO-Ca^{2+}-PCDO-II fiber are further increased to 842.6 ± 59.4 MPa and 15.8 ± 1.5 MJ m^{-3}, respectively, which are 6.0 and 3.8 times higher than that of neat rGO fiber with tensile strength of 140 MPa and toughness of 4.1 MJ m^{-3}.[2] This dramatic enhancement is attributed to the synergistic interface interactions of ionic and covalent bonding between adjacent GO nanosheets.

The mechanical properties of rGO-Ca^{2+}-PCDO-I, rGO-Ca^{2+}-PCDO-II, rGO-Ca^{2+}-PCDO-III, and rGO-Ca^{2+}-PCDO-IV fibers with different PCDO contents are compared in Figure 3b,c,

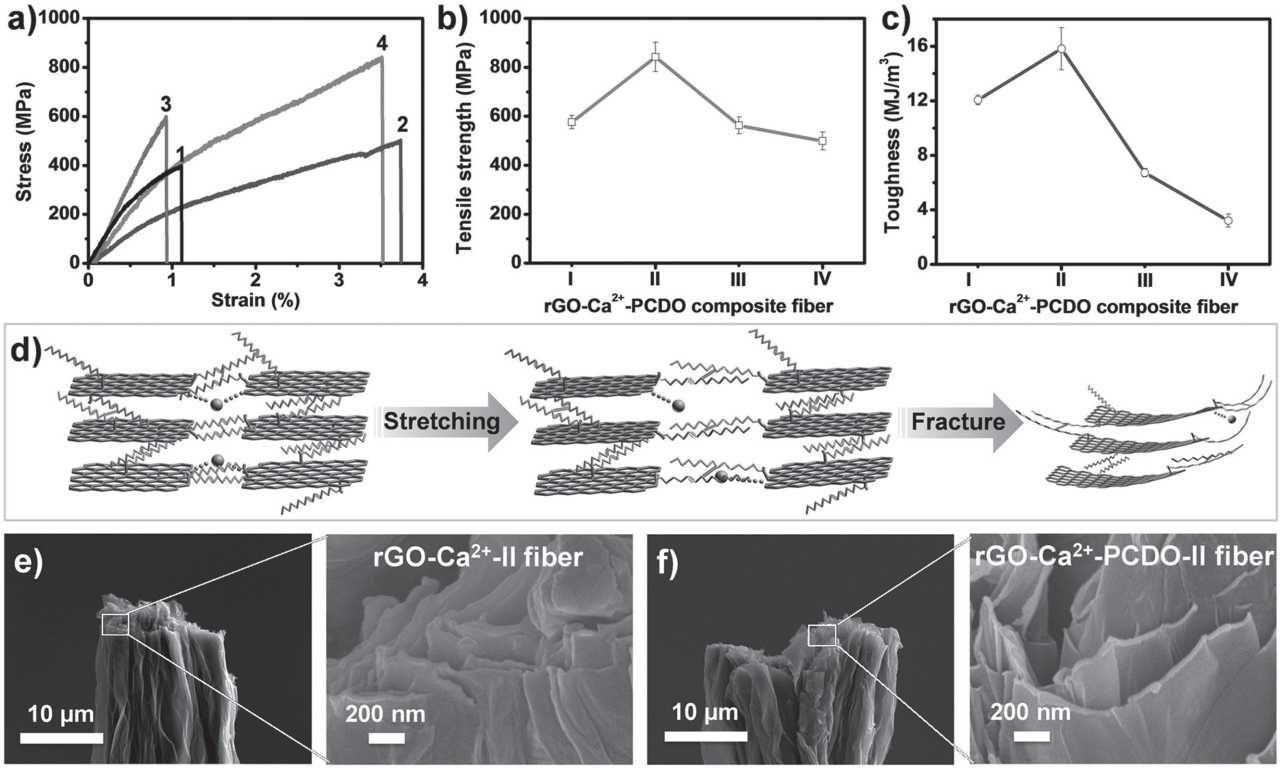

Figure 3. a) Typical stress–strain curves of GO-Ca^{2+}-II fiber (Curve 1), rGO-Ca^{2+}-II fiber (Curve 2), GO-Ca^{2+}-PCDO-II fiber (Curve 3), and rGO-Ca^{2+}-PCDO-II fiber (Curve 4). b,c) The strength and toughness of bioinspired rGO-Ca^{2+}-PCDO fiber with different PCDO contents. rGO-Ca^{2+}-PCDO-II fiber reaches the maximum values of tensile strength and toughness at the PCDO content of 3.61 wt%. d) The proposed fracture mode of bioinspired rGO-Ca^{2+}-PCDO fiber under stretching. In the early stage of the stretching process, the coiled PCDO molecules are stretched along the direction of stress. With increased loading, the bridge of ionic bonding between adjacent rGO nanosheets appears to break. Finally, the covalent bonds between PCDO molecules and rGO nanosheets start to fracture, further absorbing much more energy. Then, the external force induces the curling of the rGO nanosheet edges. e) The fracture morphology of rGO-Ca^{2+}-II fiber shows the smooth surface of rGO nanosheets. f) rGO-Ca^{2+}-PCDO-II fiber shows the pullout of rGO nanosheets with curled edge morphology.

and listed in detail in Table S5 in the Supporting Information. In this work, rGO-Ca^{2+}-PCDO-II composite fiber reached the maximum value of tensile strength and toughness at the PCDO content of 3.61 wt%. When PCDO content in GBFs was adjusted via controlling the annealing temperature, the tensile strength and toughness of the bioinspired rGO-Ca^{2+}-PCDO fibers decreased. For example, when the annealing temperature reached 160 °C, the functional groups on the GO nanosheets started to decompose, destroying the interface interactions of ionic and covalent bonding. Thus, the tensile strength and toughness of bioinspired rGO-Ca^{2+}-PCDO-IV fiber dramatically decreased, lower than those of GO-Ca^{2+}-II fiber.

The proposed fracture mode of bioinspired rGO-Ca^{2+}-PCDO fiber is illustrated to understand the synergistic toughening mechanism of ionic and covalent bonding, as shown in Figure 3d. Upon stressing, the coiled PCDO molecules were stretched along the direction of tensile stretching, triggering the slippage of adjacent rGO nanosheets in the bioinspired GBFs and resulting in significant strain and energy dissipation. With gradually increased loading, the bridge of ionic bonding between adjacent rGO nanosheets began to break, absorbing the fracture energy. When the load was further increased, the covalent bonds between PCDO molecules and rGO nanosheets started to fracture. This fracturing of covalent bonds will further absorb energy and enhance the tensile strength of bioinspired GBFs. Unlike rGO-Ca^{2+}-II fiber, bioinspired rGO-Ca^{2+}-PCDO-II fiber is characterized by the pullout of rGO nanosheets with curled-edge morphology, as shown in Figure 3e,f. This verifies the presence of covalent bonding between rGO nanosheets through PCDO molecules.[15] Side views of the cross-sections of other GO-Ca^{2+}-PCDO and rGO-Ca^{2+}-PCDO fibers are shown in Figure S12 and S13 in the Supporting Information.

Bioinspired GBFs demonstrate a record high tensile strength of 842.6 MPa, which is superior to all reported GBFs, including GBFs fabricated with different methods, ion cross-linking GBFs, and polymer reinforced GBFs, as shown in **Figure 4**. The pink area in Figure 4 shows representative GBFs assembled with different methods. For example, the first reported rGO-0 fiber assembled by the wet-spinning process[2] exhibited tensile strength of only 140 MPa, toughness of 4.1 MJ m^{-3}, and electrical conductivity of 250 S cm^{-1}. On the other hand, rGO-1 fiber assembled by a one-step dimensionally confined hydrothermal strategy with an annealing temperature of 800 °C achieved a tensile strength of 420 MPa but a low electrical conductivity of 10 S cm^{-1}. When thermally treated at a high temperature of 1500 °C,[19] the obtained rGO-2 fiber displayed a tensile strength of 378 MPa, a toughness of only 1.89 MJ m^{-3}, and a high electrical conductivity of 285 S cm^{-1}. BGFs prepared

Adv. Mater. 2016,
DOI: 10.1002/adma.201506074

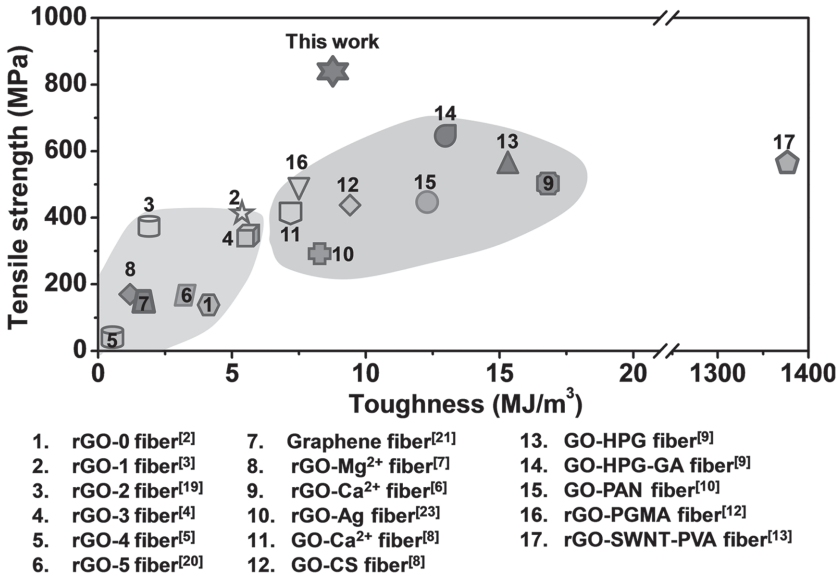

Figure 4. Comparison of tensile strength and toughness of bioinspired rGO-Ca^{2+}-PCDO-II fiber, along with other GBFs with different ionic bonding and polymer reinforcement, indicating that the tensile strength of the bioinspired rGO-Ca^{2+}-PCDO-II fiber is higher than that of all reported GBFs to date.

by other methods, such as "programmable writing" (rGO-4 fiber),[4] rGO-5 fiber,[20] and scrolling graphene film,[21] are impossible to go over 400 MPa in tensile strength, far lower than that of bioinspired GBFs.

Compared with crosslinked divalent ions,[6,7] the tensile strength of bioinspired GBFs is 5.1 and 1.7 times higher than that of rGO-Mg^{2+} fiber[7] and rGO-Ca^{2+} fiber,[6] respectively. Polymer-reinforced GBFs show improved mechanical properties. For example, rGO–single-walled carbon nanotubes (SWNTs)–PVA fiber[22] synergistically reinforced with PVA between rGO nanosheets and SWNTs shows high toughness of 1380 MJ m^{-3}, which is higher than that of bioinspired GBFs with toughness of 15.8 MJ m^{-3}. The low toughness of bioinspired GBFs is likely caused by the fact that the cross-linking of PCDO enhances the tensile strength and limits the slippage of rGO nanosheets under loading, resulting in the relatively low absorption of fracture energy in the stress process. However, the tensile strength of rGO-SWNT-PVA fiber is only 570 MPa, lower than the reported maximum tensile strength of 652 MPa for GBFs such as GO-HPG-GA,[9] and even lower than that of bioinspired GBFs with tensile strength of 842.6 MPa. The detailed mechanical properties of all these GBFs are listed in Table S6 in the Supporting Information. Due to their excellent tensile strength and toughness, this kind of bioinspired graphene-based fiber can be twirled into knots without fracture and also be hanged a two grams of weight without breakage, as shown in Figure S14 in the Supporting Information, and the corresponding videos are shown in Movie S1 and S2 in the Supporting Information.

In addition to their excellent mechanical properties, bioinspired rGO-Ca^{2+}-PCDO fibers are also promising for their excellent electrical conductivity as high as 292.4 S cm^{-1} (Table S7, Supporting Information), which is superior to those of previous neat rGO fibers and other GBFs with high polymer content, such as rGO-HPG fibers,[9] rGO-PVA fibers,[11] and rGO-PGMA fibers.[12] Although silver particle-doped GO fibers (rGO-Ag fibers[23] show high electrical conductivity of 930 S cm^{-1}, the tensile strength of rGO-Ag fiber is only 300 MPa, less than half of the tensile strength of the bioinspired GBFs.

In conclusion, inspired by the abundant interfacial interactions of natural nacre, we have demonstrated ultrastrong graphene-based fibers via synergistic interactions of ionic and covalent bonding. The tensile strength of this bioinspired GBF reaches up to 842.6 MPa, the highest ever recorded. In addition, this bioinspired GBF has high electrical conductivity of 292.4 S cm^{-1}. These unique properties make bioinspired GBF a great candidate for applications in flexible electrodes for supercapacitors, aerospace, artificial muscles, wearable, and intelligent devices, including actuators, motors, and robots. This bioinspired synergistic toughening strategy also creates a promising avenue for constructing robust and highly conductive GBFs in the near future.

Experimental Section

Materials: Graphene oxide nanosheets were synthesized from the neat natural graphite powder by the previously reported modified Hummer's method. The 57 wt% HI acid was purchased from Sigma–Aldrich, and PCDO was purchased from Tokyo Chemical Industry Co., Ltd.

Fabrication of Bioinspired rGO-Ca^{2+}-PCDO Fibers: The GO-Ca^{2+} fibers were obtained by the reported wet-spinning method. The spinning dopes (≈10 mg mL^{-1}) were loaded into a 1 mL plastic syringe with a spinning nozzle (PEEK tube with a diameter of 130 μm), and the as-prepared spinning dopes were continuously injected into the rotating coagulation baths with diameter of 12.5 cm (10 rpm) at a rate of 30 μL min^{-1} (about 4 m min^{-1}). The coagulation baths were ethanol–water (1:3 v:v) solutions containing 5 wt% $CaCl_2$. The GO-Ca^{2+} fibers were immersed in the coagulation baths for 30 min and then transferred into the washing bath (ethanol–water solution) to wash off the residual salts. The washed GO-Ca^{2+} fibers were then convolved onto the wire loop. The collected wet GO-Ca^{2+} fibers were air-dried at room temperature. Then, the GO-Ca^{2+} fibers were annealed at 40, 80, 120, and 160 °C in an oven under an air atmosphere for 3 h, respectively. The annealed GO-Ca^{2+} fibers were immersed into the PCDO/tetrahydrofuran solution for grafting PCDO onto the GO nanosheets. Subsequently, the GO-Ca^{2+}-PCDO fibers were treated under UV irradiation at a wavelength of 365 nm to cross-link the PCDO molecules. The obtained GO-Ca^{2+}-PCDO fibers were immersed into the HI solution for 12 h to remove the residual functional groups from the GO nanosheets. After washing iodine away with ethanol, the ultrastrong bioinspired rGO-Ca^{2+}-PCDO fibers were finally obtained.

Characterization: The mechanical properties were measured in the tensile mode using a Shimadzu AGS-X Tester at a loading rate of 0.2 mm min^{-1} with a gauge length of 5 mm. All fibers were cut with the length of 20 mm before measuring. The results for each sample are based on the average value of ≈3–5 specimens. Scanning electron microscopy (SEM) images were obtained using a field-emission scanning electron microscope (JEOL-7500F and Quanta 250 FEG). The TGA was measured using a Netzsch TG 209F1 Libra, NSK under nitrogen with a rate of temperature increase of 10 °C min^{-1}. XRD profiles were collected using Cu K_α radiation (λ = 1.54 nm). XPS was performed using ESCALab220i-XL (Thermo Scientific) with the X-ray source of a monochromatic Al K_α.

Raman spectroscopy was conducted using a Renishawin Via Plus Raman microscope. The electrical conductivities of the GBFs were measured by a standard two-probe method using a source meter.

Supporting Information

Supporting Information is available from the Wiley Online Library or from the author.

Acknowledgments

Y.Y.Z., Y.C.L., and M.P. contributed equally to this work. This work was supported by the Excellent Young Scientist Foundation of NSFC (51522301), the National Natural Science Foundation of China (21273017, 51103004), the Program for New Century Excellent Talents in University (NCET-12-0034), the Beijing Nova Program (Z121103002512020), the Fok Ying-Tong Education Foundation (141045), the Open Project of Beijing National Laboratory for Molecular Sciences, the 111 Project (B14009), the Aeronautical Science Foundation of China (20145251035, 2015ZF21009), the State Key Laboratory for Modification of Chemical Fibers and Polymer Materials, Donghua University (LK1508), and the Fundamental Research Funds for the Central Universities (YWF-15-HHXY-001).

Received: December 7, 2015
Revised: December 25, 2015
Published online:

[1] a) Z. Xu, C. Gao, *Mater. Today* **2015**, *18*, 480; b) F. Meng, W. Lu, Q. Li, J.-H. Byun, Y. Oh, T.-W. Chou, *Adv. Mater.* **2015**, *27*, 5113; c) Z. Xu, C. Gao, *Acc. Chem. Res.* **2014**, *47*, 1267.
[2] Z. Xu, C. Gao, *Nat. Commun.* **2011**, *2*, 571.
[3] Z. Dong, C. Jiang, H. Cheng, Y. Zhao, G. Shi, L. Jiang, L. Qu, *Adv. Mater.* **2012**, *24*, 1856.
[4] J. Cao, Y. Zhang, C. Men, Y. Sun, Z. Wang, X. Zhang, Q. Li, *ACS Nano* **2014**, *8*, 4325.
[5] R. Cruz-Silva, A. Morelos-Gomez, H. I. Kim, H. K. Jang, F. Tristan, S. Vega-Diaz, L. P. Rajukumar, A. L. Elias, N. Perea-Lopez, J. Suhr, M. Endo, M. Terrones, *ACS Nano* **2014**, *8*, 5959.
[6] Z. Xu, H. Sun, X. Zhao, C. Gao, *Adv. Mater.* **2013**, *25*, 188.
[7] X. Hu, Z. Xu, C. Gao, *Sci. Rep.* **2012**, *2*, 767.
[8] R. Jalili, S. H. Aboutalebi, D. Esrafilzadeh, R. L. Shepherd, J. Chen, S. Aminorroaya-Yamini, K. Konstantinov, A. I. Minett, J. M. Razal, G. G. Wallace, *Adv. Funct. Mater.* **2013**, *23*, 5345.
[9] X. Hu, Z. Xu, Z. Liu, C. Gao, *Sci. Rep.* **2013**, *3*, 2374.
[10] Z. Liu, Z. Xu, X. Hu, C. Gao, *Macromolecules* **2013**, *46*, 6931.
[11] L. Kou, C. Gao, *Nanoscale* **2013**, *5*, 4370.
[12] X. Zhao, Z. Xu, B. Zheng, C. Gao, *Sci. Rep.* **2013**, *3*, 3164.
[13] U. G. Wegst, H. Bai, E. Saiz, A. P. Tomsia, R. O. Ritchie, *Nat. Mater.* **2015**, *14*, 23.
[14] a) G. Q. Xin, T. K. Yao, H. T. Sun, S. M. Scott, D. L. Shao, G. K. Wang, J. Lian, *Science* **2015**, *349*, 1083; b) M. Zhang, Y. Wang, L. Huang, Z. Xu, C. Li, G. Shi, *Adv. Mater.* **2015**, *27*, 6708; c) H. Bai, F. Walsh, B. Gludovatz, B. Delattre, C. Huang, Y. Chen, A. P. Tomsia, R. O. Ritchie, *Adv. Mater.* **2016**, *28*, 50; d) S. Wan, J. Peng, Y. Li, H. Hu, L. Jiang, Q. Cheng, *ACS Nano* **2015**, *9*, 9830; e) S. Wan, Y. Li, J. Peng, H. Hu, Q. Cheng, L. Jiang, *ACS Nano* **2015**, *9*, 708; f) S. Gong, W. Cui, Q. Zhang, A. Cao, L. Jiang, Q. Cheng, *ACS Nano* **2015**, *9*, 11568; g) Q. Cheng, J. Duan, Q. Zhang, L. Jiang, *ACS Nano* **2015**, *9*, 2231.
[15] Q. Cheng, M. Wu, M. Li, L. Jiang, Z. Tang, *Angew. Chem., Int. Ed.* **2013**, *52*, 3750.
[16] H.-K. Jeong, Y. P. Lee, M. H. Jin, E. S. Kim, J. J. Bae, Y. H. Lee, *Chem. Phys. Lett.* **2009**, *470*, 255.
[17] S. Pei, J. Zhao, J. Du, W. Ren, H.-M. Cheng, *Carbon* **2010**, *48*, 4466.
[18] S. Park, K.-S. Lee, G. Bozoklu, W. Cai, S. T. Nguyen, R. S. Ruoff, *ACS Nano* **2008**, *2*, 572.
[19] C. Xiang, N. Behabtu, Y. Liu, H. G. Chae, C. C. Young, B. Genorio, D. E. Tsentalovich, C. Zhang, D. V. Kosynkin, J. R. Lomeda, C.-C. Hwang, S. Kumar, M. Pasquali, J. M. Tour, *ACS Nano* **2013**, *7*, 1628.
[20] H. P. Cong, X. C. Ren, P. Wang, S. H. Yu, *Sci. Rep.* **2012**, *2*, 613.
[21] J. Sun, Y. Li, Q. Peng, S. Hou, D. Zou, Y. Shang, Y. Li, P. Li, Q. Du, Z. Wang, *ACS Nano* **2013**, *7*, 10225.
[22] M. K. Shin, B. Lee, S. H. Kim, J. A. Lee, G. M. Spinks, S. Gambhir, G. G. Wallace, M. E. Kozlov, R. H. Baughman, S. J. Kim, *Nat. Commun.* **2012**, *3*, 650.
[23] Z. Xu, Z. Liu, H. Sun, C. Gao, *Adv. Mater.* **2013**, *25*, 3249.